

Article

Quantifying the Unwinding due to Ram Pressure Stripping in Simulated Galaxies

Rubens E. G. Machado , Caroline F. O. Grinberg  and Elvis A. Mello-Terencio 

Departamento Acadêmico de Física, Universidade Tecnológica Federal do Paraná, Av. Sete de Setembro 3165, Curitiba, Brazil

* Correspondence: rubensmachado@utfpr.edu.br

Abstract: Galaxies moving through the gas of the intracluster medium (ICM) experience ram pressure stripping, which can leave behind a gas tail. When a disk galaxy receives the wind edge-on, however, the characteristic signature is not a typical jellyfish tail, but rather an unwinding of the spiral arms. We aim to quantify such asymmetries both in the gas and in the stellar component of a simulated galaxy. To this end, we simulate a gas-rich star-forming spiral galaxy moving through a self-consistent ICM gas. The amplitude and location of the asymmetries were measured via Fourier decomposition. We found that the asymmetry is much more evident in the gas component, but it is also measurable in the stars. The amplitude tends to increase with time and the asymmetry radius migrates inwards. We found that, when considering the gas, the spiral arms extend much further and are more unwound than the corresponding stellar arms. Characterizing the unwinding via simulations should help inform the observational criteria used to classify ram pressure stripped galaxies, as opposed to asymmetries induced by other mechanisms.

Keywords: galactic dynamics; spiral galaxies; numerical simulations; intracluster medium

1. Introduction

Galaxies are affected by their environment. When a gas-rich galaxy travels through the gas of the Intracluster Medium (ICM), it can be stripped of its Interstellar Medium (ISM) gas by the phenomenon of ram pressure [1]. This removal of gas may contribute to the quenching of star formation and thus it can have significant effects on the evolution of the galaxy [2].

The morphology of the galaxy is also affected by ram pressure. In extreme cases, a long trail of gas may be left behind. These are known as jellyfish galaxies. To a partial degree, jellyfish-like tails are commonly observed in cluster galaxies. The survey GAS Stripping Phenomena in galaxies (GASP) has been carrying out an intensive program of observations to study ram pressure in galaxies [3–5].

From the simulation point of view, the ram pressure mechanism has been often studied under various conditions, to explore star formation, the effects of inclinations, gas content, orbits etc [6–10]. Jellyfish galaxies have also been studied within cosmological simulations of galaxy formation, for example, with IllustrisTNG [11–13] and EAGLE [14,15].

Recently, the peculiar feature of the ‘unwinding’ of the spiral arms has been pointed out in the literature by Bellhouse et al. [16]. This description of the morphology refers to the shape of the spiral arms, which apparently tend to become more sheared and stretched. This unwinding can be more clearly noticed when the galaxy is seen face-on. Moreover, the configuration which maximizes the unwinding phenomenon is presumably the one where the galaxy receives the wind edge-on. Thus, one side of the disk develops more trailing and open spiral arms, than the side which is moving towards the wind. The layout most favorable to unwinding is the opposite of the more canonical jellyfish configuration. In a classical jellyfish, we see the disk edge-on, while it receives the wind face-on. In this



Citation: Machado, R. E. G.; Grinberg, C. F. O.; Mello-Terencio, E. A.

Quantifying the unwinding due to ram pressure stripping in simulated galaxies. *Galaxies* **2025**, *1*, 0.

<https://doi.org/>

Received: 20 May 2025

Revised: 19 June 2025

Accepted: 03 July 2025

Published:



Copyright: © 2025 by the authors. Licensee MDPI, Basel, Switzerland. This article is an open access article distributed under the terms and conditions of the Creative Commons Attribution (CC BY) license (<https://creativecommons.org/licenses/by/4.0/>).

setting, the galaxy develops a tail ideally perpendicular to the disk itself. The unwinding morphology is therefore less conspicuous than a classical jellyfish. Additionally, it may be confused with tidal tails, which are gravitational in nature; while the origin of the ram pressure induced unwinding is hydrodynamical.

In hindsight, such unwinding morphology had indeed manifested itself in a few simulation works [17–19]. In Schulz and Struck [17], it was noticed that spirals in the outer disk stretch and shear. In Roediger et al. [18], a simulated galaxy with edge-on wind develops strong asymmetry. In Steinhauser et al. [19], a degree of asymmetry is also noticeable.

Observationally, probable unwinding candidates had been seen in [20–23]. Expanding on the topic, Vulcani et al. [24] performed a visual inspection of *B*-band images and identified 143 galaxies with unwinding features. More recently, George et al. [25] presented a prominent example of a strong ram pressure stripped galaxy with unwinding spiral arms, along with additional candidates from GASP. Krabbe et al. [26] presented methods for finding ram pressure stripped galaxies, and obtained 33 candidates, of which one third showed clear evidence of unwinding arms. Crossett et al. [27] employed citizen science classifications to identify ram pressure stripped galaxies, and found that those galaxies have a significantly lower than average arm winding with respect to comparison samples.

Galactic disks may become asymmetric for various other reasons, generally related to tidal interactions. For example, lopsided galaxies are described as having a distortion where one a side of the disk is more elongated than the other [28]; galaxies exhibiting lopsidedness are commonly observed and also studied in simulations. One of the interests in studying the ram pressure induced unwinding is to disentangle the different mechanisms that could lead to similar observed asymmetries. The unwinding of the spiral arms displays morphological features which are reminiscent of typical tidal tails. However, there may be characteristic signatures which would discriminate between the different mechanisms. These signatures may be in the kinematics, stellar ages or gas morphology.

In this paper, we aim to characterize the properties of a simulated galaxy undergoing ram pressure stripping. In particular, our goal is to quantify the global asymmetry that develops in the galactic disk, and also to explore the phenomenon of the unwinding of the spiral arms. This paper is organized as follows. In section 2 we describe the simulation setup. In section 3 we present the results of our analyses. We conclude with a summary in section 4.

2. Simulation

In order to study the phenomenon of ram pressure stripping, we carried out a hydrodynamical *N*-body simulation of a spiral galaxy falling into a cluster. The initial conditions of both the galaxy and the cluster will be described in the following.

The galaxy consists of a stellar disk, a gas disk, a bulge and a dark matter halo. The stellar disk follows an exponential profile:

$$\rho_d(R, z) = \frac{M_d}{4\pi R_d^2 z_d} \exp\left(-\frac{R}{R_d}\right) \text{sech}^2\left(\frac{z}{z_d}\right), \quad (1)$$

where $M_d = 5 \times 10^{10} M_\odot$ is the mass of the disc, $R_d = 3.5$ kpc is the radial scale length, and $z_d = 0.7$ kpc is the vertical scale length. For the gas disk, the radial scale length is the same, but the vertical scale length is $z_g = 0.035 z_d$. The initial mass of the gas disk is $M_g = 2 \times 10^{10} M_\odot$. The bulge and the dark matter halo both follow a Hernquist [29] density profile. The halo mass and scale length are $M_h = 1 \times 10^{12} M_\odot$ and $a_h = 47$ kpc. For the bulge, $M_b = 1 \times 10^{10} M_\odot$ and $a_b = 1.5$ kpc. These choices of parameters result in a galaxy vaguely similar to the Milky Way.

Fig. 1 presents the circular velocity curves for the galaxy initial conditions, separated into the components: halo, disk, gas, bulge, and total. The Toomre parameter for the stellar disk is also presented in Fig. 1. The method to generate the initial conditions follows the prescription of Springel et al. [30], where the ratio of radial to vertical velocity dispersions

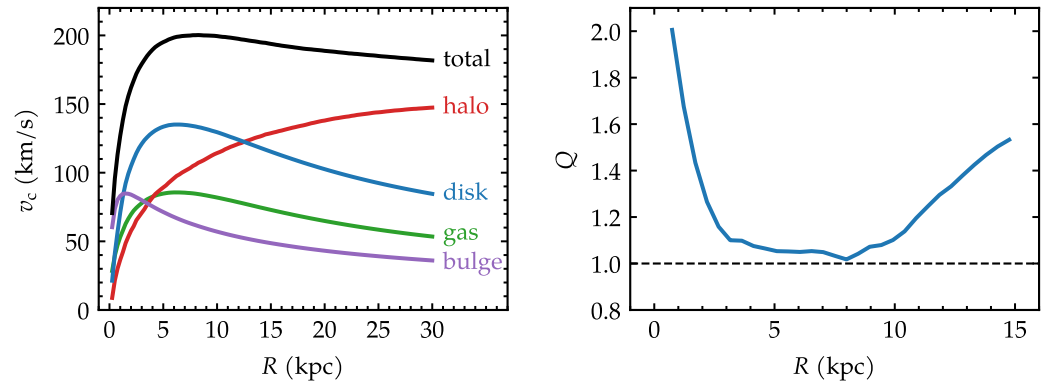


Figure 1. Left: Circular velocity curves for the galaxy initial conditions. Right: Toomre parameter of the stellar disk in the initial conditions.

$f_R = \sigma_R^2 / \sigma_z^2$ is a free parameter. We adopted the choice of $f_R = 0.8$ as in Ruggiero and Lima Neto [31], which leads to a relatively stable disc in isolation. In practice, numerical transients occur but dissipate mostly within the first 0.1 Gyr.

A common approach to simulate ram pressure would be to insert the galaxy into an idealized wind tunnel [6,7]. This approach is more computationally cost-effective but tends to be generally more idealized. Nevertheless, it is possible to set up wind tunnels that emulated the radial density profile of the ICM. Simulating the full ICM self-consistently is another approach that is sometimes adopted [19,31]. While it has the advantage of being naturally more realistic, it also much more costly due to the considerable total volume of the ICM. In this work, we opt to create the initial conditions of a self-consistent galaxy cluster. This spherically symmetric galaxy cluster consist of two components: dark matter halo and gas. Both components are represented by the Hernquist [29] profile. The dark matter halo has $M_h = 9 \times 10^{13} M_\odot$ and $a_h = 280$ kpc. The ICM gas has $M_g = 1 \times 10^{13} M_\odot$ and also $a_g = 280$ kpc. This choice of parameters leads to a galaxy cluster with a dense cool core and a gas fraction of 10%.

The initial conditions for the galaxy and for the cluster were created using, respectively, the GALSTEP¹ and the CLUSTEP² codes [31]. Realizations were made with the following numbers of particles for the galaxy: $N_d = 1 \times 10^5$, $N_g = 1 \times 10^5$, $N_b = 2 \times 10^4$ and $N_h = 2 \times 10^5$, for the disk, gas, bulge and halo, respectively. The cluster was created with $N_h = 5 \times 10^6$ particles in the halo and $N_g = 5 \times 10^6$ particles in the gas component. These choices imply that the gas component is more finely resolved, which is desirable in the context of the present work. Furthermore, this translates into a mass resolution of $m_g = 2 \times 10^5 M_\odot$ for the gas particles in the galaxy, and $m_g = 2 \times 10^6 M_\odot$ for the gas particles in the cluster. In this multiscale setup, we are faced with a wide dynamical range between the mass of the galaxy and the mass of the cluster. Thus, the computational cost of a fixed mass resolution across all particles would have been exceedingly challenging in practice.

The mass resolution of this simulation may be contrasted to those in IllustrisTNG simulations, a well established state-of-the-art simulation suite in the field. For instance, TNG100 adopts a baryonic mass resolution of $1.4 \times 10^6 M_\odot$ [32], and has been successfully used to study jellyfish galaxies, including detailed analyses of ram pressure interactions between the interstellar medium and intracluster medium, as well as the resulting morphological signatures [11]. Yet, important caveats remain. The sensitivity of galactic dynamics to numerical resolution is a common concern. For example, Sellwood [33,34] showed how

¹ <https://github.com/elvismello/galstep>

² <https://github.com/elvismello/clustep>

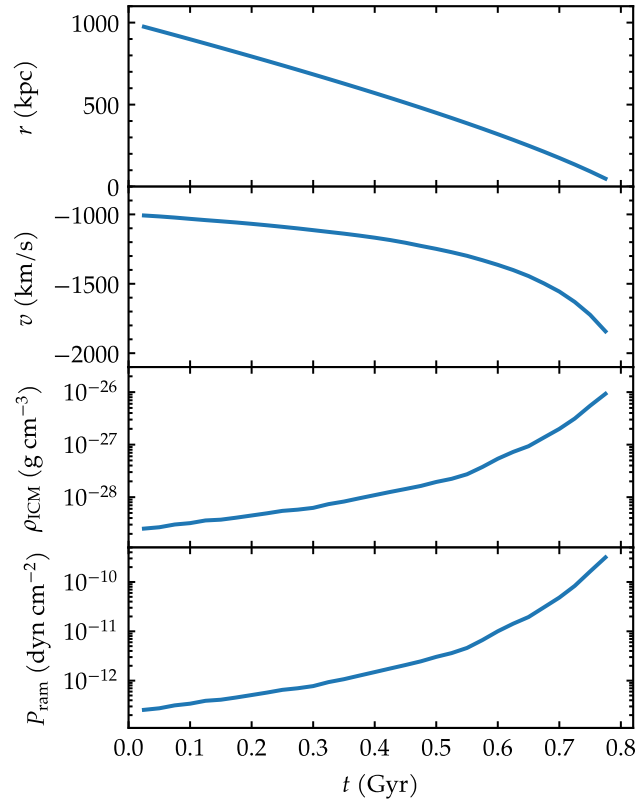


Figure 2. Orbital evolution of the galaxy. The first and second panels display the radial position and the velocity of the galaxy. The third and fourth panels show the density of the ICM gas it encounters, and the corresponding ram pressure.

particle resolution can significantly affect secular processes such as bar formation and disk heating. Moreover, even in high-resolution cosmological simulations such as TNG50 [35], some dynamical phenomena remain insufficiently captured. One example is the so-called fast bar tension discussed in [36], which persists in TNG50 but appears to be alleviated in the higher-resolution Auriga simulations [37]. Thus, while our adopted resolution is consistent with values commonly used in the field, this does not eliminate the possibility of numerical effects on small-scale dynamics. A systematic convergence study is deferred to a future work.

At the start of the simulation ($t = 0$), the galaxy is placed at $x = 1000$ kpc, with a velocity of $v_x = -1000$ km s⁻¹ entirely along the x axis. In other words, the galaxy is set to fall in a radial orbit towards the center of the cluster. Since the galactic disk lies on the xy plane, and the velocity vector of the galaxy is confined to the same plane, this means that the galaxy will receive the wind always edge-on throughout the simulation.

The simulation is performed with Gadget-3, a version of the Gadget-2 code [38] including star formation. The maximum integration time step was 0.001 Gyr. Before the simulation starts, the dark matter particles of the cluster are excised from the snapshot. Instead, the gravitational potential of the cluster halo is represented by a frozen analytic potential with the exact same parameters as the N -body realization. This is justified by the fact that, during the evolution, the dark matter of the cluster will not be significantly altered by the passage of the galaxy. Replacing the N -body particles by an analytic potential reduces computational cost.

The simulation is carried out for 1 Gyr, which is roughly the time required for the galaxy to traverse the radius of the cluster. More precisely, the first two panels of Fig. 2 indicate the evolution of the orbital parameters of the galaxy, namely its clustercentric distance and its radial velocity as a function of time. Throughout the paper, the time evolution will be generally presented up to $t \sim 0.8$ Gyr at most, or shortly earlier. At later

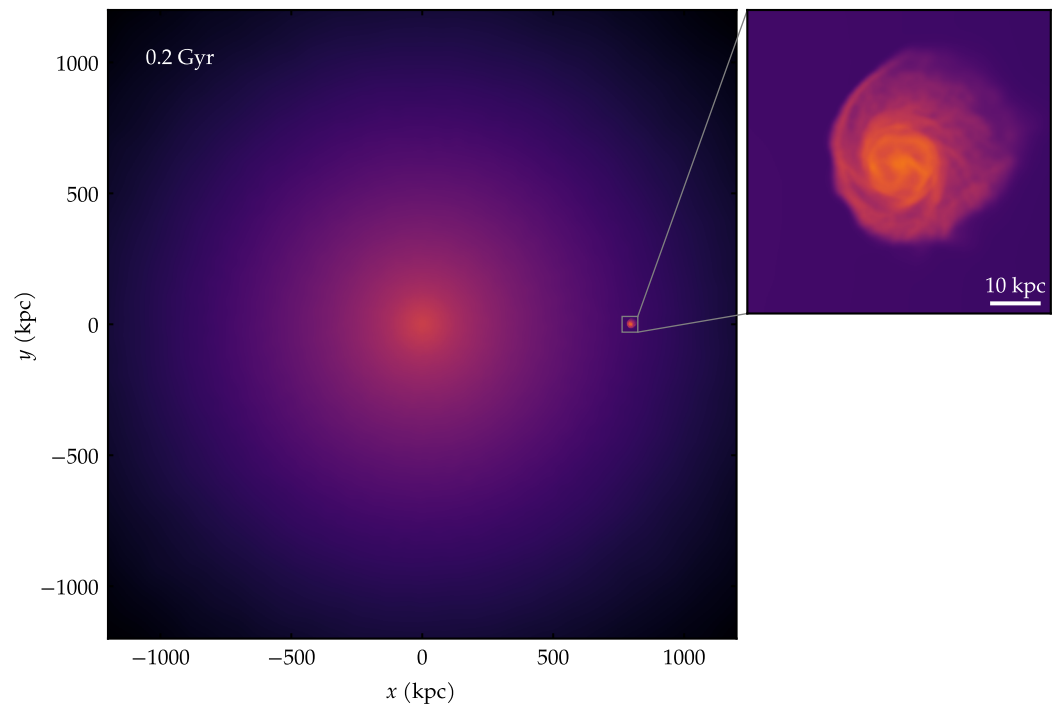


Figure 3. Map of projected gas density showing the galaxy falling into the cluster, at $t = 0.2$ Gyr.

times, the galaxy would cross the very center of the potential well, leading to unphysical consequences. Therefore, our discussions are limited to the infall from $r = 1000$ kpc until the galaxy reaches about $r \sim 100$ kpc.

As the galaxy travels towards the center, it meets progressively denser gas. Fig. 2 also displays the density of the ICM gas which is encountered by the galaxy at each time in its trajectory, as well as the ram pressure that acts on the galaxy. From the gas density ρ_{ICM} and the wind velocity v , the ram pressure is computed as:

$$P_{\text{ram}} = \rho_{\text{ICM}} v^2. \quad (2)$$

An illustrative visualization of the galaxy in the presence of the cluster environment is given in Fig. 3, where the colors represent the gas density of both components together, ISM and ICM. This example is shown at $t = 0.2$ Gyr, by which time the galaxy has already fallen a few 100 kpc. The zoomed-in inset panel in Fig. 3 helps underscore the disparity of spatial scales involved in this problem.

3. Analysis and results

3.1. Global evolution

The effects of ram pressure become noticeable as soon as the simulation starts — mildly at first, and then strongly as time progresses. Fig. 4 exhibits the morphological evolution of the gas and of the stars, at selected times. In this and in all other subsequent visualizations of the paper, the origin of the coordinate system has been shifted to coincide with the center of the galaxy. In the reference frame of the galaxy, the wind direction is to be understood as arriving from the left towards the right. This wind direction is constant throughout the simulation and is shown as a green arrow in one of the panels of Fig. 4.

Already at $t = 0.1$ Gyr, the leftmost side of the gas disk is undergoing a subtle but noticeable amount of compression. At the same time, the stellar disk remains fairly axisymmetric. Between 0.1 and 0.5 Gyr, the ram pressure grows steadily, and as a result the gas disk becomes clearly asymmetric. This is seen in the upper set of frames in Fig. 4. The gradual unwinding of the spiral arms is qualitatively perceptible from this visualization.

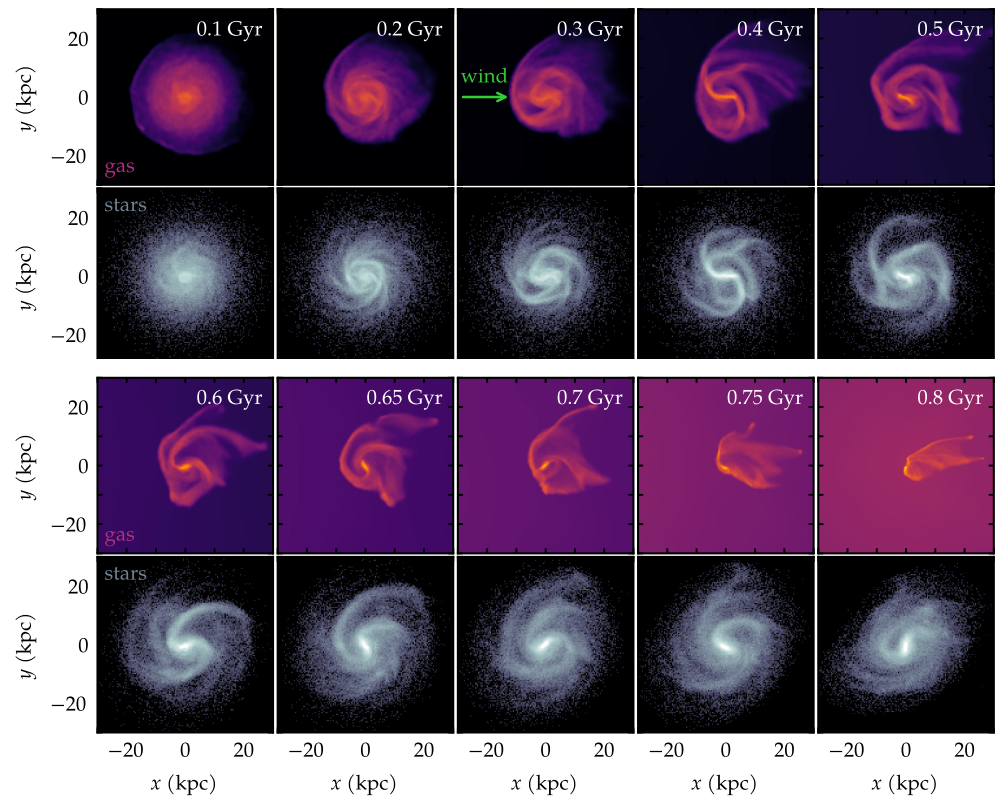


Figure 4. Maps of projected density of gas and stars at selected times during the evolution. Notice that the background ICM gas is also shown. The green arrow represents the constant wind direction.

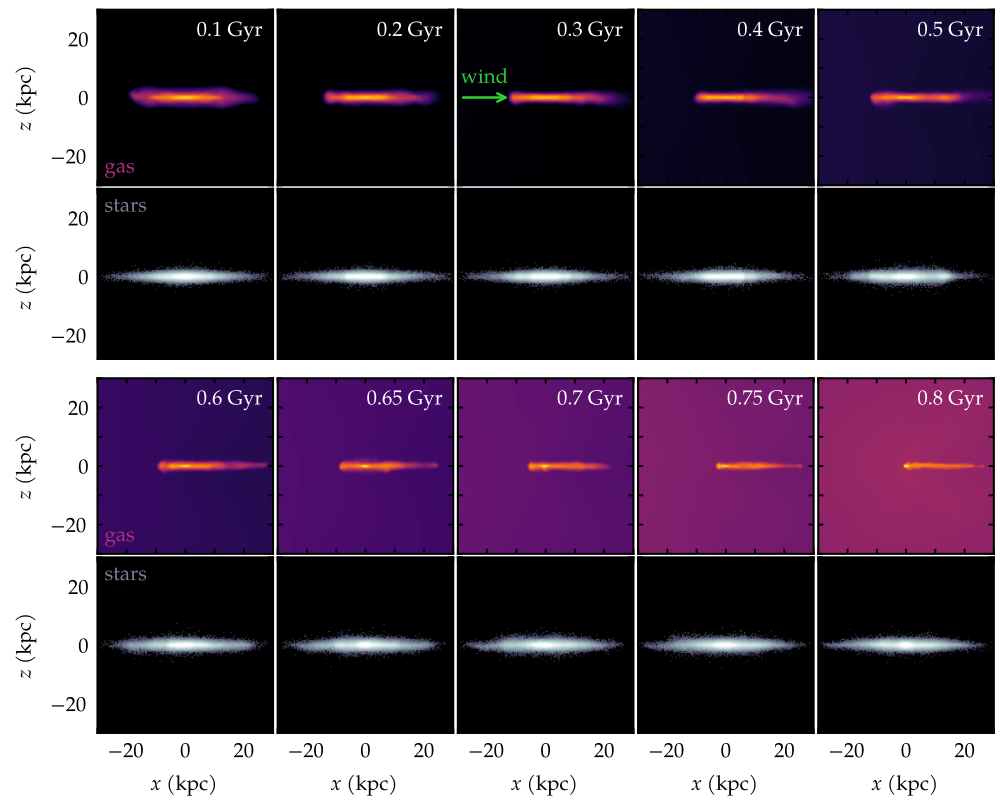


Figure 5. Same as Fig. 4 but showing an edge-on view.

In the lower set of frames in Fig. 4, selected times are shown in the range from 0.6 to 0.8 Gyr. This later phase corresponds to a distinct regime. Firstly, the time scale itself is naturally shorter, due to the acceleration of the galaxy. The evolution of the velocity seen in Fig. 2 indicates that this is the phase of greatest acceleration, as the galaxy approaches the core of the cluster. Likewise, both the density and the ram pressure are intensified at this final phase. According to Fig. 2, after about $t \sim 0.55$ Gyr, there is a marked change in the slope of the evolution of ρ_{ICM} and of P_{ram} . By this time, the galaxy has already travelled some ~ 600 kpc. Yet, during the remaining ~ 300 kpc, it will experience an increase of ram pressure more pronounced than in the earlier phase. The consequence of this extreme ram pressure is seen in the 0.6–0.8 Gyr gas panels of Fig. 4. Inspection of slightly later snapshots (not shown) confirms that the gas tail seen at 0.8 Gyr will be mostly stripped away. After 0.8 Gyr, both the gas and the stars undergo distortions that would not be meaningful to interpret physically. In a real cluster in the Universe, a collision would probably have occurred with a Brightest Cluster Galaxy (BCG) by that point.

It should also be noted that the apparent asymmetry of the stellar disk towards $t \sim 0.8$ Gyr cannot be confidently attributed to ram pressure effects, and is more likely due to strong tidal forces near the cluster center. In this sense, interpretations of both the gas and the stars should be regarded with caution at the latest snapshots. For these reasons, most of the analysis will focus on the more reliable early phases. The largely unwound gas spiral arms themselves are a disturbance that could in principle have some local influence on the nearby stars. Even though the gas mass is relatively small, it may exert subtle tidal forces on the stellar arms.

Fig. 5 displays the equivalent evolution of Fig. 4, but showing an edge-on view. Since the galaxy receives the wind in a direction entirely parallel to the disk, there is no cause for vertical asymmetries. As a result, neither the gas disk nor the stellar disk develop any noticeable features in the vertical direction. The unwound spiral arms in the gas are essentially confined to the same heights as the rest of the gas disk.

3.2. Amplitude and location of the asymmetries

We wish to quantify the degree to which the morphology of the galaxy departs from an axisymmetric configuration. Strictly speaking, once spiral arms are well developed, the disk is no longer axisymmetric, even in an unperturbed galaxy. Nevertheless, the phenomenon of unwinding clearly produces a global elongation in a preferred direction. In other words, beyond a given radius, there is more material (more extended arms) in one side of the galaxy than in the opposite side. This feature is suitable to be quantified by means of a Fourier decomposition of the projected mass distribution. In particular, the $m = 1$ mode should be able to capture the signal of such an asymmetry. The relevant coefficients can be written as:

$$a_0 = \sum_{i=0}^N m_i \quad (3)$$

$$a_1 = \sum_{i=0}^N m_i \cos \theta_i \quad (4)$$

$$b_1 = \sum_{i=0}^N m_i \sin \theta_i, \quad (5)$$

where m_i is the mass of each particle and θ_i is the azimuthal angle of each particle. The summation is performed using all the N particles that fall inside a given annulus. Thus, we can define the amplitude A_1 as:

$$A_1 = \frac{\sqrt{a_1^2 + b_1^2}}{a_0} \quad (6)$$

and measure it as function of cylindrical radius R .

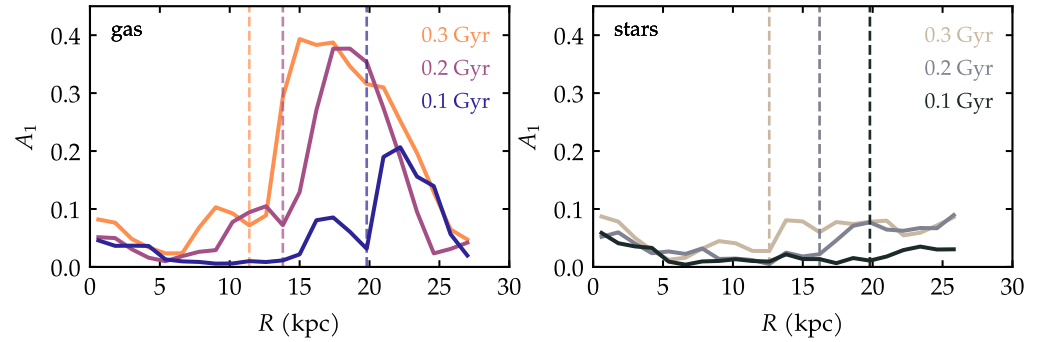


Figure 6. Radial profiles of A_1 for the gas and the stars at different times. The vertical lines correspond to the radii of the minimum value of A_1 before the peak; this is the asymmetry radius R_s .

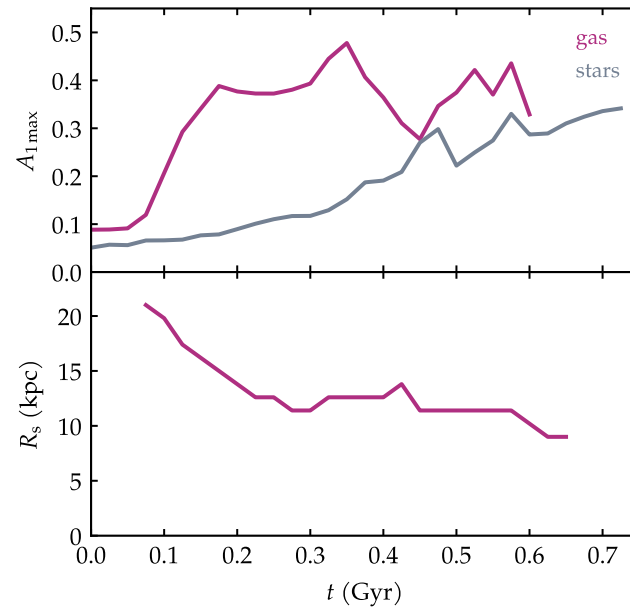


Figure 7. Top: time evolution of $A_{1\max}$ for the gas and the stars. Bottom: time evolution of the asymmetry radius, as measured from the gas.

Fig. 6 presents the results of this measurement performed for both the gas and the stars at different times. The profiles are generally noisy because this metric also captures the presence of the spiral arms themselves. Nevertheless, when a very important asymmetry is present, it is clearly seen as a peak in the radial profile of $A_1(R)$. In the left panel of Fig. 6, we see that the peaks in the gas are quite pronounced. As time progresses, the peaks seem to become higher and also move towards smaller radii. (To ensure that the asymmetry is not due to mere secular evolution, the measurement was repeated for an isolated galaxy; see Appendix A.) The location of the peaks has a direct interpretation: it is the radius of greatest asymmetry. These peaks are also useful to define a certain radius: the radius within which the galaxy is still relatively ‘symmetric’, or put another way, the radius beyond which the asymmetry becomes very pronounced — we define it as the radius R_s . This radius could be referred to as the ‘asymmetry radius’ in the sense that that is where the asymmetry begins. This radius R_s is measured in practice as the first minimum to the left of the peak of $A_1(R)$. The vertical lines in Fig. 6 mark the values of R_s obtained for the corresponding times shown in the figure.

The same procedure that was done for the gas can also be applied to the stars. This is shown in the right panel of Fig. 6. The radial profiles show that the amplitude of A_1 for the stars is much smaller, but non-zero. It is also true that the amplitude increases with time. The R_s are in principle measurable, but are ill-defined and difficult to determine.

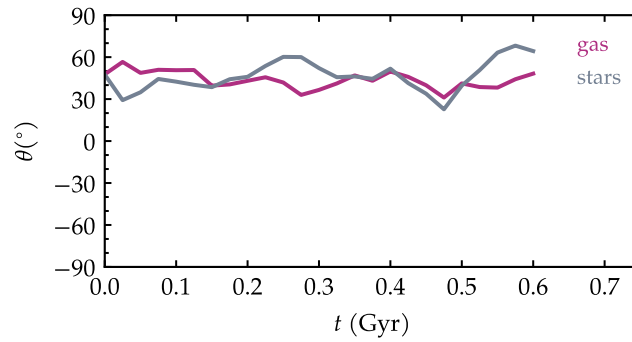


Figure 8. Direction of the elongation, as determined by the Radon transform, for both gas and stars.

At each time in the simulation, we can measure the height of the peak in the radial profile of A_1 . This is the definition of the quantity $A_{1\max}$, which is shown in the upper panel of Fig. 7, for gas and stars. Here we see a more quantitative characterization of the asymmetries and their evolutions. The asymmetry of the stars is smaller and evolves slowly. The asymmetry of the gas is more pronounced and grows quickly in the beginning of the simulation. At later times, the comparison becomes less conclusive. At times when the morphology of the spiral arms is extremely irregular and peculiar, A_1 captures these signatures rather than the intended global asymmetry.

The evolution of the asymmetry radius R_s is shown in the lower panel of Fig. 7 only from the gas measurements, because in the stellar component the profiles of $A_1(R)$ are too noisy to find R_s reliably. It is interesting to notice that R_s decreases with time. This means that, at first, the asymmetry is manifested only in the outskirts of the disk, while most of the galaxy remains relatively symmetric. As time progresses, the asymmetry radius migrates inward, meaning that now a larger part of the outer disk is disturbed as well.

3.3. Direction of the elongation

The galactic disk undergoing ram pressure under these conditions is no longer circular, but rather elongated. The elongation is somewhat analogous to the ‘tail’ of a jellyfish. However, in a more classical jellyfish, the tail is generally expected to point in the direction opposite to the direction of motion of the galaxy; it is a wake of material left behind. In the edge-on case analyzed here, a striking feature seen in the morphology of all snapshots is that the major axis of this elongation is not parallel to the wind direction. Instead, there is an angle between the direction of the wind and the direction of the elongation. This angle seems to be roughly constant and seems to be connected to the sense of rotation of the galaxy.

In order to quantify the direction of the elongation, we chose to apply a Radon transform, a tool occasionally used in Astronomy [39]; see footnotes in [40]. The Radon transform of an image results in a so-called ‘sinogram’ whose most intense projection gives the preferred direction. The definition is given in Appendix B. This was measured as a function of time for both gas maps and stellar maps. The results are shown in Fig. 8. The general conclusion is that the elongation (i.e. the ‘tail’ equivalent) of the galaxy points roughly $\sim 45^\circ$ away from the motion of the galaxy. The measurement of this angle is likewise hindered by the irregularity of the spiral arms themselves, resulting in a relatively broad dispersion of some $\pm 10^\circ$ around the average over time. Nevertheless, it is remarkable that the elongation is consistently confined to (the middle of) the first quadrant. In all visualization images in this paper, the rotation of the galaxy is counter-clockwise. It seems consistent that the leading edges of the spiral arms become preferentially compressed when they meet the wind in the second quadrant.

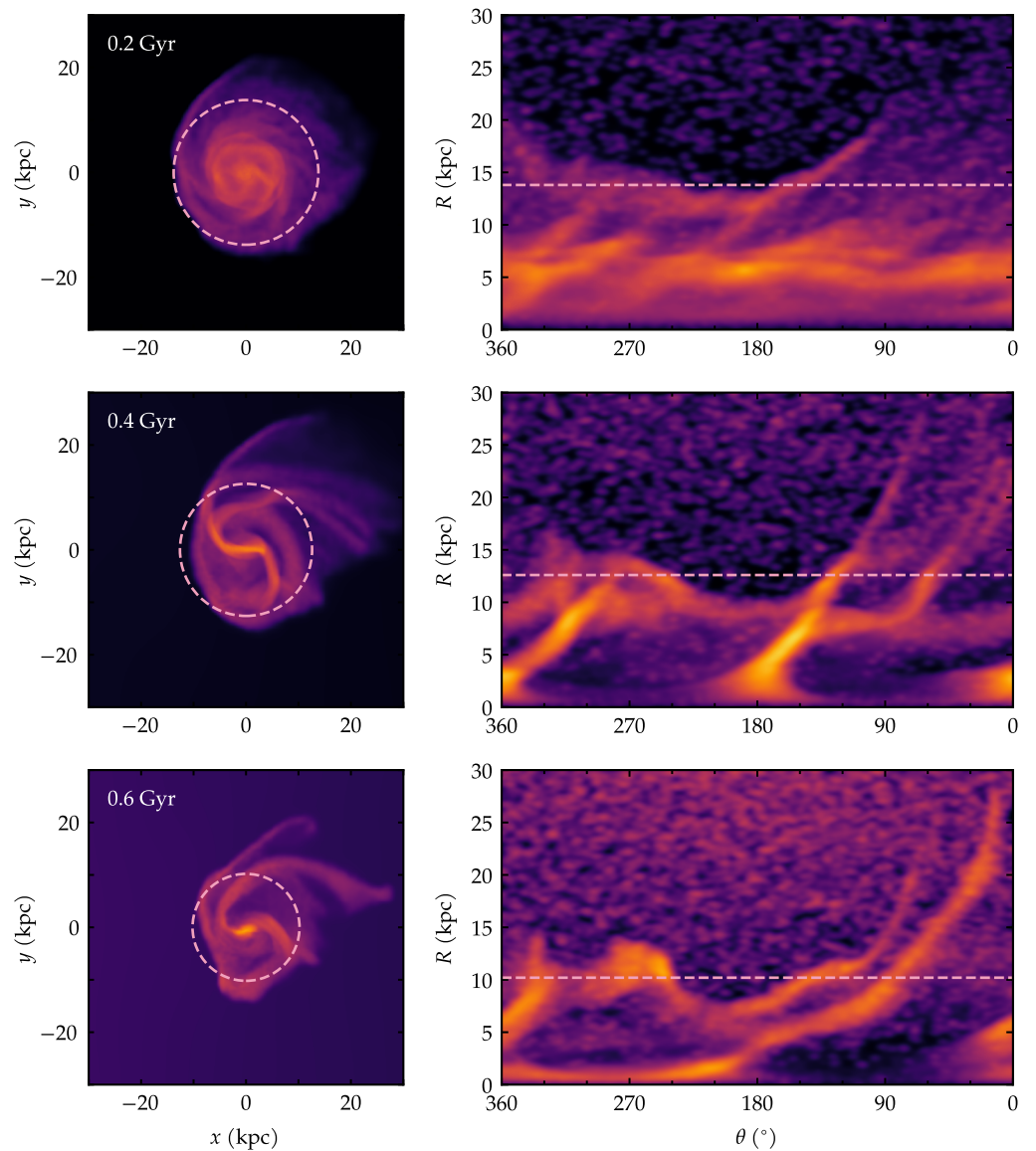


Figure 9. Left: maps of projected gas density. Right: azimuthal plots at the corresponding times. The circles and the horizontal lines correspond to the asymmetry radius R_s .

3.4. Shapes of the spiral arms

Finally, in order to scrutinize the shapes of the spiral arms more closely, we unwrap the azimuthal coordinate in the form of rectangular plots of the polar coordinates: R as a function of θ . This is shown separately for the gas in Fig. 9, and for the stars in Fig. 10. Accompanying the azimuthal plots are normal density maps of the galaxy at the corresponding times. The dashed pink circles overlaid on the density maps correspond to the asymmetry radius R_s . It is noticeable in the gas maps of Fig. 9 that the circles indeed enclose the region which could be considered relatively symmetric, thus highlighting the outer region which clearly lacks symmetry.

In the stellar density maps of Fig. 10, the same pink circles are shown, i.e. the same R_s measured from the gas, not the stars. As had been pointed out earlier, even though the stellar asymmetry can be quantitatively detected by A_1 , it is not qualitatively visible by eye.

Turning to the azimuthal plots on the right panels of Fig. 9, the corresponding values of R_s naturally translate into a line of constant radius in the $R - \theta$ plot. This helps guide the view of the outermost part of the galaxy, where the asymmetries are most important.

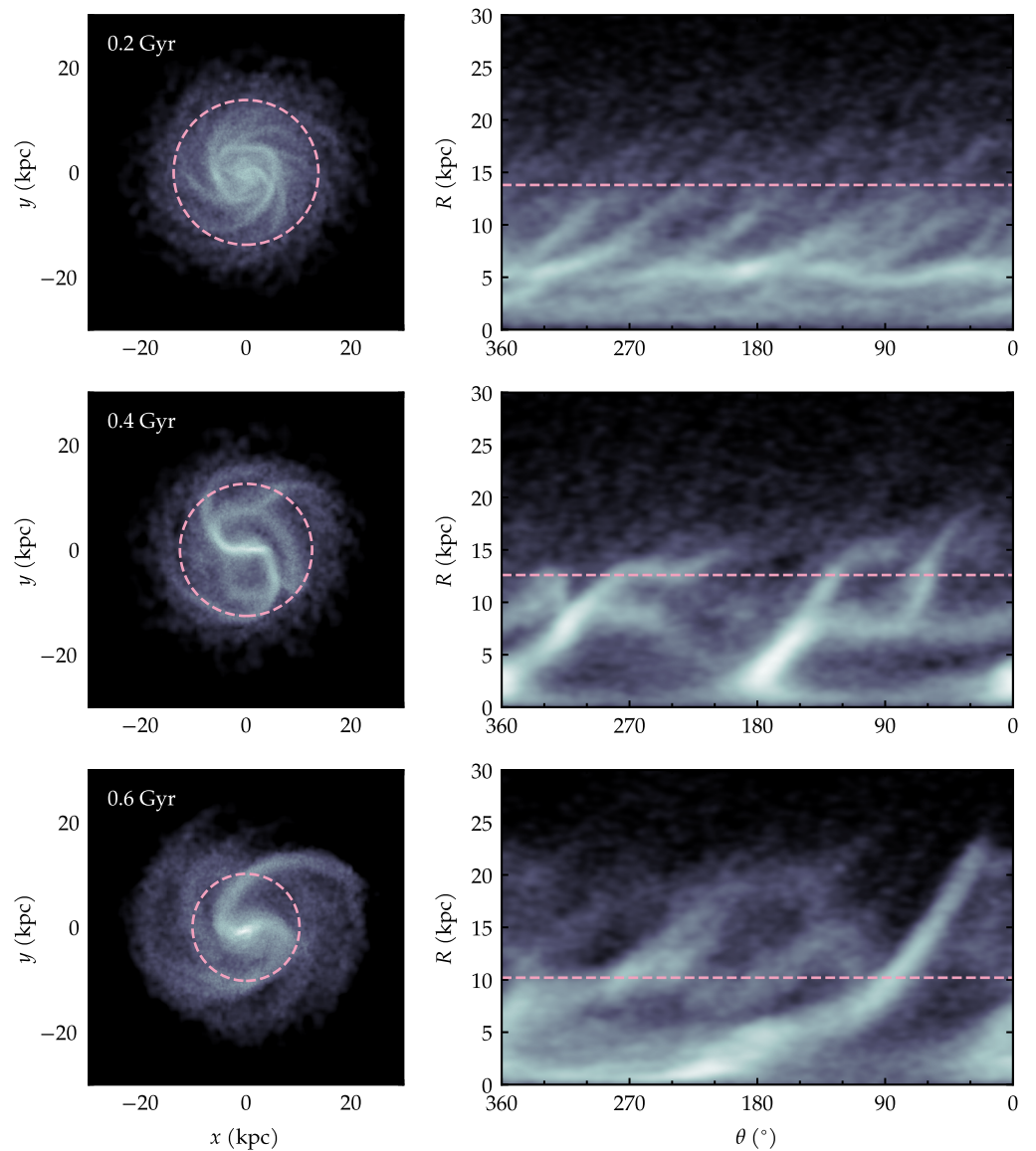


Figure 10. Left: maps of projected stellar density. Right: azimuthal plots at the corresponding times. The circles and the horizontal lines correspond to the asymmetry radius R_s .

The horizontal axes of the azimuthal plots are shown counter-clockwise (from 360° to 0°), to help guide the eye as one follows a given spiral arm along its azimuths. One can read these plots in the following manner. If a given spiral arm were very tightly wound — or in the limiting case, if it were a ring — then, as one reads its azimuths, it would trace a region of roughly constant R , i.e. a flat feature in the $R - \theta$ plot. On the other hand, a very open unwound arm reaches increasingly larger values of R as one sweeps its azimuths; thus an unwinding arm translates into an upward branch in the $R - \theta$ plot.

With this interpretation in mind, we can appreciate in Fig. 9 the progressive unwinding of the arms. At first, at $t = 0.2$ Gyr, there is hardly any upward branch in the azimuthal plot, apart from a short segment peaking above the dashed line. At $t = 0.4$ Gyr, there are tenuous but very long branches reaching up above the dashed line. At $t = 0.6$ Gyr, there are stronger branches. Notice that the preferential region for the upward branches is the first quadrant (i.e. between 90° and 0°). This is consistent with the general elongation of the galaxy being confined to this quadrant, as seen in the previous subsection.

Now, contrasting the gas to the stars of Fig. 10, we find interesting differences. At $t = 0.2$ Gyr, there are no unwinding branches, just common spiral arms covering azimuths uniformly. At $t = 0.4$ Gyr, we see that there is a correspondence between the main arms in gas and in stars. However, the faint thin tendrils seen in the gas are missing in the stars. At $t = 0.6$ Gyr, one arm is present in the gas but absent in the stars; another arm extends further in the gas, while it is truncated sooner in the stars.

The nature of these features is confirmed when comparing directly the density maps Figs. 9 and 10. We find that within the circle of radius R_s , there is a general match between spiral arms seen in the gas and in the stars. However, beyond R_s there are clear departures in the gas, whose arms extends much further and are more unwound than the corresponding stellar arms.

4. Discussion

In this paper, we have analyzed a hydrodynamical simulation in which a galaxy falls into a cluster, encountering the wind edge-on. In this configuration, the ram pressure causes the spiral arms to unwind. During the first phase of the infall, the ram pressure builds up gradually, stripping the gas and causing the gas to become noticeably asymmetric. At a later phase, as the galaxy approaches the denser gas in the core of the cluster, the ram pressure steepens significantly and the spiral arms in the gas are swept away almost completely. Meanwhile, the effects on the stellar disk are more subtle.

We have quantified the amplitude and the location of the asymmetries by a Fourier decomposition of the projected mass. We found that the asymmetry is much stronger in the gas, but it is also detectable in the stellar disk as well. The amplitude of the asymmetry generally increases over time. In the case of the stars, this evolution is slow and mild. In the case of the gas, the asymmetry grows steeply in the beginning.

Furthermore, we quantified the radius beyond which the asymmetries are most important. In general, the phenomenon of ram pressure tends to impact first the gas in the periphery of the disk, which is more precariously bound to the galactic potential. That is also the case here. The asymmetry radius is large at first, meaning that only the outskirts beyond 20 kpc are affected in the first phase. At later times, this radius migrates inwards to 10 kpc, showing that a relevant fraction of the disk is perturbed.

Even though the galaxy was set to move along the x axis, we found that the direction of the elongation (analogous to a ‘tail’) was on average at an angle of $\sim 45^\circ$ with respect to the line of motion. This is consistent with the findings of Bellhouse et al. [16]. This tail direction depends of the motion of the galaxy and also on its sense of rotation, as on one side the leading part or the arms moves against the wind, and on the the other side, with the wind. This results is potentially interesting to clarify the probable direction of the trail vectors in certain jellyfish galaxies. In the case of galaxies the receive the wind face-on, the direction of the tail is generally interpreted as pointing in the direction opposite to the velocity vector of the galaxy. In the case of a ram pressure stripped galaxy moving edge-on, the direction of motion is less clear.

Following the approach of Bellhouse et al. [16], we employed azimuthal diagrams in order to characterize the unwinding of the spiral arms. This is a useful tool to inspect the morphological evolution of the spiral arms. We found that the upward branches in the diagrams, representing the unwinding arms, are the longest and the most intense in the first quadrant. Additionally, the features in the gas are seen to extend further than in the stars.

In comparison to previous works, the type morphology that arises in our simulations is qualitatively similar. For example, Schulz and Struck [17] had seen arms that were stretched and sheared. Roediger and Brüggen [6,41] had simulated galaxies undergoing ram pressure under different inclinations and found a strong degree of asymmetry in the xy plane in an equivalent wind configuration. Such noticeable edge-on stripping was also presente in Roediger et al. [18]. It is interesting to notice that the conditions under which such asymmetry develope are apparently broad. More quantitatively, the analysis

of Bellhouse et al. [16] further explored the detailed morphology of the spiral arms, both in observations and in simulations. Our simulation confirms that a galaxy falling into a self-consistent cluster will develop a similar degree of unwinding in the gas, as seen from the azimuthal diagrams.

A relevant issue to address is the question of why the stellar component should be affected at all, since ram pressure is in principle a purely hydrodynamical effect. In this regard, the main effect expected to be at play is star formation. Since the gas is continually forming stars in the simulation, star formation takes place also in the recently disturbed gas spiral arms. For this reason, the stellar spiral arms should be at least partially perturbed, although the bulk of the older stellar population would remain mostly undisturbed. This expectation is in line with the results of Bellhouse et al. [16], who find predominantly young stars in the unwound component. A secondary effect might also contribute to the stellar asymmetries, to a lesser degree. When the gas disk is strongly stripped by ram pressure, this redistribution of mass may affect the stellar component through their mutual gravity. This has been suggested by ram pressure simulations [42] in which the stellar disk is temporarily deformed, and even the central region of the dark matter halo becomes slightly offset. Such indirect effects might also play a role in perturbing the stellar spiral arms in the edge-on wind case.

The environment through which the galaxy travels determines the impact of the ram pressure stripping. This is why the specific orbits are important [43]. In this paper, only one galaxy trajectory was considered, namely a radial orbit; and only one inclination, edge-on. These choices were made in order to obtain a configuration in which the effect of interest would be most pronounced. Moreover, the density profile of the ICM gas exhibits a dense cool core. By design, these environmental and orbital properties all contribute towards our simulated galaxy having undergone a particularly intense history of ram pressure stripping.

5. Conclusions

Our conclusions can be summarized as follows. (i) A galaxy receiving the wind edge-on undergoes unwinding of the spiral arms. In agreement with previous works, we find that this phenomenon occurs naturally in this circumstance. Additionally, we confirm that the direction of the tail tends to be on average at an angle of $\sim 45^\circ$. (ii) This work extends the analysis to the stellar component as well. We find that the unwinding of the spiral arms is also measurable in the stars, although it is much more noticeable in the gas. In the case of the gas, arms extend further out and are more unwound.

In future simulations, it would be interesting to explore the unwinding phenomenon in galaxies moving along different environments and receiving the wind under varied inclinations. In particular, the present analysis could be repeated for populations of different stellar ages, in order to confirm the expected predominance of young stars in the unwound component. From a theoretical standpoint, these kinds of simulations can be used to explore in greater detail the dynamics of the gas to understand how the velocities in the spiral arms are impacted by the compression of the gas. Furthermore, this paper was focused on the density of the gas and stellar components. In order to offer a closer connection to observations, a useful perspective would be to produce mock images in specific observational bands and in $H\alpha$. These would help with the interpretation of the observations of ram pressure stripped galaxies exhibiting unwinding of the spiral arms.

Author Contributions: Conceptualization, RM; methodology, RM, CG, EMT; software, RM, CG, EMT; formal analysis, RM, CG; resources, RM; writing—original draft preparation, RM; writing—review and editing, RM; visualization, RM; supervision, RM; project administration, RM; funding acquisition, RM. All authors have read and agreed to the published version of the manuscript.

Funding: RM acknowledges support from the Brazilian agency *Conselho Nacional de Desenvolvimento Científico e Tecnológico* (CNPq) through grants 406908/2018-4, 303426/2018-7, and 307205/2021-5 and from *Fundação Araucária* through grant PDI 346/2024 – NAPI *Fenômenos Extremos do Universo*. CG

acknowledges support from *Coordenação de Aperfeiçoamento de Pessoal de Nível Superior - Brasil (CAPES)* – Finance Code 001. EMT acknowledges support from UTFPR.

Data Availability Statement: The original data can be shared upon reasonable request to the corresponding author.

Acknowledgments: The authors acknowledge the National Laboratory for Scientific Computing (LNCC/MCTI, Brazil) for providing HPC resources of the SDumont supercomputer, which have contributed to the research results reported within this paper.

Conflicts of Interest: The authors declare no conflicts of interest. The funders had no role in the design of the study; in the collection, analyses, or interpretation of data; in the writing of the manuscript; or in the decision to publish the results.

Appendix A. Isolated galaxy

An isolated galaxy could in principle develop some degree of asymmetry due to its own internal secular evolution. To ensure that the peaks of A_1 seen in Fig. 6 are indeed caused by the ram pressure unwinding, the same measurements were performed using an isolated galaxy. This galaxy is an identical initial condition, but evolved in a vacuum, i.e. in the absence of the ICM environment. The morphological evolution of the isolated galaxy is seen in Fig. A1. It undergoes some numerical transients in the first moments. The isolated galaxy does develop some mild intrinsic asymmetries detectable via the A_1 (Fig. A2), but they are considerably smaller than in the stripped galaxy. This confirms that the peaks of A_1 in Fig. 6 are indeed capturing the asymmetries that were seen in the gas morphology.

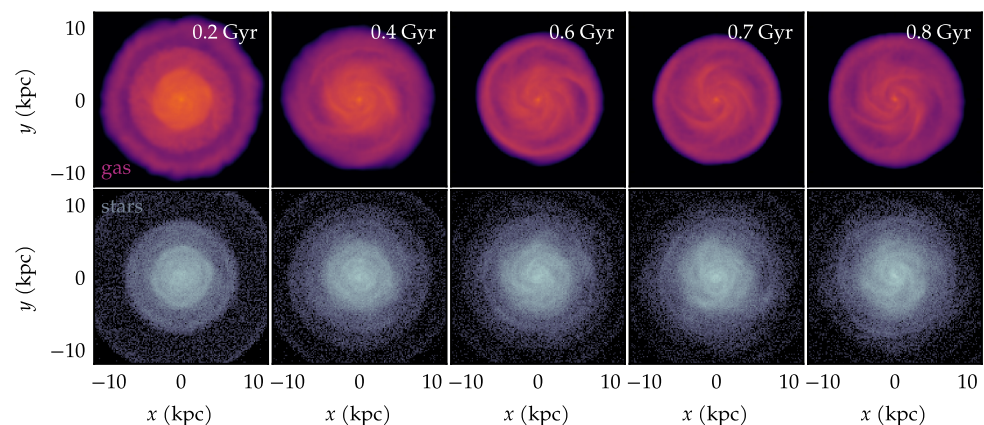


Figure A1. The evolution of the isolated galaxy, showing the gas and stars at selected times.

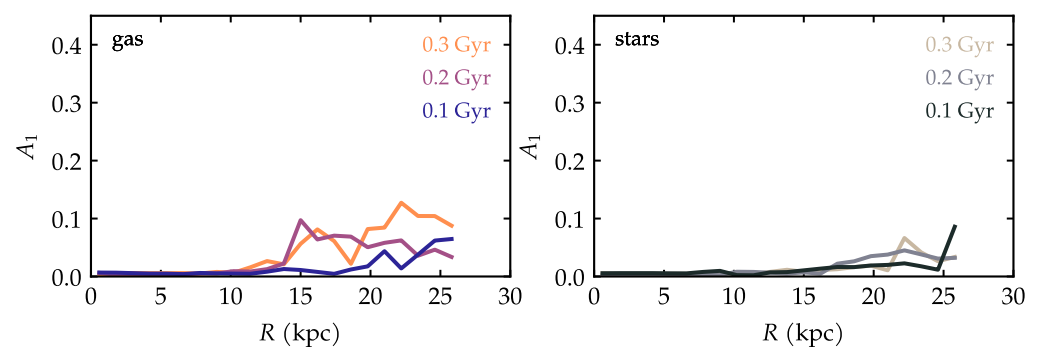


Figure A2. Same as Fig. 6, but for the isolated galaxy.

Appendix B. The Radon transform

The Radon transform of a function $f(x, y)$ in two dimensions is defined as the line integrals of $f(x, y)$ over all lines L (see [39,40] and references therein):

$$\tilde{f} = \int_L f(x, y) ds, \quad (\text{A1})$$

It takes a function defined in two-dimensional space (typically an image), and transforms it into (p, θ) space:

$$\tilde{f}(p, \phi) = \int_{-\infty}^{\infty} f(p \cos \phi - s \sin \phi, p \sin \phi + s \cos \phi) ds, \quad (\text{A2})$$

corresponding to a set of projections of that function along different directions, with each value equal to the line integral of the function over that line.

When applied to the image of a galaxy, the angle for which the Radon transform yields the highest response provides a good estimation for the direction of greatest elongation. An illustrative example is shown in Fig. A3.

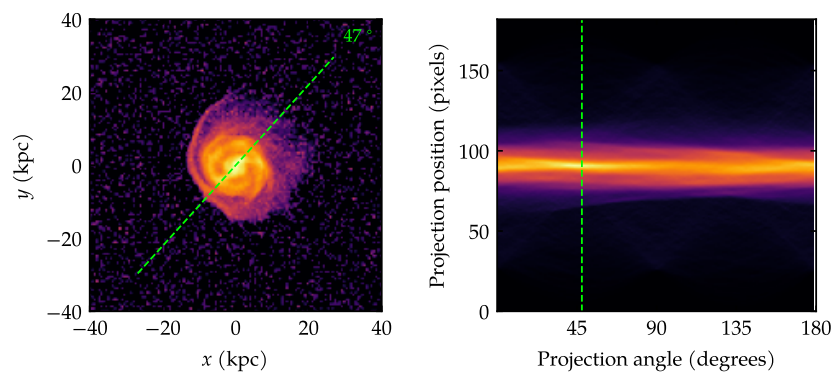


Figure A3. Illustrative example of the application of the Radon transform. Left: Gas density map of the galaxy at 0.22 Gyr. Right: Sinogram showing the result of the Radon transform as a function of projection angle. The dashed green lines correspond to the maximum response (right) and thus to the orientation of the galaxy (left) in this example.

References

1. Gunn, J.E.; Gott, J. Richard, I. On the Infall of Matter Into Clusters of Galaxies and Some Effects on Their Evolution. *Astrophys. J.* **1972**, *176*, 1. <https://doi.org/10.1086/151605>.
2. Boselli, A.; Fossati, M.; Sun, M. Ram pressure stripping in high-density environments. *Astron. Astrophys. Rev.* **2022**, *30*, 3, [arXiv:astro-ph.GA/2109.13614]. <https://doi.org/10.1007/s00159-022-00140-3>.
3. Poggianti, B.M.; Moretti, A.; Gullieuszik, M.; Fritz, J.; Jaffé, Y.; Bettoni, D.; Fasano, G.; Bellhouse, C.; Hau, G.; Vulcani, B.; et al. GASP. I. Gas Stripping Phenomena in Galaxies with MUSE. *Astrophys. J.* **2017**, *844*, 48, [arXiv:astro-ph.GA/1704.05086]. <https://doi.org/10.3847/1538-4357/aa78ed>.
4. Gullieuszik, M.; Poggianti, B.M.; Moretti, A.; Fritz, J.; Jaffé, Y.L.; Hau, G.; Bischko, J.C.; Bellhouse, C.; Bettoni, D.; Fasano, G.; et al. GASP. IV. A Muse View of Extreme Ram-pressure-stripping in the Plane of the Sky: The Case of Jellyfish Galaxy JO204. *Astrophys. J.* **2017**, *846*, 27, [arXiv:astro-ph.GA/1708.09035]. <https://doi.org/10.3847/1538-4357/aa8322>.
5. Jaffé, Y.L.; Poggianti, B.M.; Moretti, A.; Gullieuszik, M.; Smith, R.; Vulcani, B.; Fasano, G.; Fritz, J.; Tonnesen, S.; Bettoni, D.; et al. GASP. IX. Jellyfish galaxies in phase-space: an orbital study of intense ram-pressure stripping in clusters. *Mon. Not. R. Astron. Soc.* **2018**, *476*, 4753–4764, [arXiv:astro-ph.GA/1802.07297]. <https://doi.org/10.1093/mnras/sty500>.
6. Roediger, E.; Brüggén, M. Ram pressure stripping of disc galaxies: the role of the inclination angle. *Mon. Not. R. Astron. Soc.* **2006**, *369*, 567–580, [arXiv:astro-ph/0512365]. <https://doi.org/10.1111/j.1365-2966.2006.10335.x>.
7. Tonnesen, S.; Bryan, G.L. Star formation in ram pressure stripped galactic tails. *Mon. Not. R. Astron. Soc.* **2012**, *422*, 1609–1624, [arXiv:astro-ph.CO/1203.0308]. <https://doi.org/10.1111/j.1365-2966.2012.20737.x>.
8. Steinhauser, D.; Haider, M.; Kapferer, W.; Schindler, S. Galaxies undergoing ram-pressure stripping: the influence of the bulge on morphology and star formation rate. *Astron. Astrophys.* **2012**, *544*, A54, [arXiv:astro-ph.CO/1208.1265]. <https://doi.org/10.1051/0004-6361/201118311>.

9. Tonnesen, S.; Bryan, G.L. It's Cloud's Illusions I Recall: Mixing Drives the Acceleration of Clouds from Ram Pressure Stripped Galaxies. *Astrophys. J.* **2021**, *911*, 68, [arXiv:astro-ph.GA/2102.05061]. <https://doi.org/10.3847/1538-4357/abe7e2>.
10. Akerman, N.; Tonnesen, S.; Poggianti, B.M.; Smith, R.; Marasco, A. How Ram Pressure Drives Radial Gas Motions in the Surviving Disk. *Astrophys. J.* **2023**, *948*, 18, [arXiv:astro-ph.GA/2301.09652]. <https://doi.org/10.3847/1538-4357/acbf4d>.
11. Yun, K.; Pillepich, A.; Zinger, E.; Nelson, D.; Donnari, M.; Joshi, G.; Rodriguez-Gomez, V.; Genel, S.; Weinberger, R.; Vogelsberger, M.; et al. Jellyfish galaxies with the IllustrisTNG simulations - I. Gas-stripping phenomena in the full cosmological context. *Mon. Not. R. Astron. Soc.* **2019**, *483*, 1042–1066, [arXiv:astro-ph.GA/1810.00005]. <https://doi.org/10.1093/mnras/sty3156>.
12. Joshi, G.D.; Pillepich, A.; Nelson, D.; Marinacci, F.; Springel, V.; Rodriguez-Gomez, V.; Vogelsberger, M.; Hernquist, L. The fate of disc galaxies in IllustrisTNG clusters. *Mon. Not. R. Astron. Soc.* **2020**, *496*, 2673–2703, [arXiv:astro-ph.GA/2004.01191]. <https://doi.org/10.1093/mnras/staa1668>.
13. Rohr, E.; Pillepich, A.; Nelson, D.; Zinger, E.; Joshi, G.D.; Ayromlou, M. Jellyfish galaxies with the IllustrisTNG simulations - when, where, and for how long does ram pressure stripping of cold gas occur? *Mon. Not. R. Astron. Soc.* **2023**, *524*, 3502–3525, [arXiv:astro-ph.GA/2304.09196]. <https://doi.org/10.1093/mnras/stad2101>.
14. Troncoso-Iribarren, P.; Padilla, N.; Santander, C.; Lagos, C.D.P.; García-Lambas, D.; Rodríguez, S.; Contreras, S. The better half - asymmetric star formation due to ram pressure in the EAGLE simulations. *Mon. Not. R. Astron. Soc.* **2020**, *497*, 4145–4161, [arXiv:astro-ph.GA/2001.06501]. <https://doi.org/10.1093/mnras/staa274>.
15. Kulier, A.; Poggianti, B.; Tonnesen, S.; Smith, R.; Ignesti, A.; Akerman, N.; Marasco, A.; Vulcani, B.; Moretti, A.; Wolter, A. Ram Pressure Stripping in the EAGLE Simulation. *Astrophys. J.* **2023**, *954*, 177, [arXiv:astro-ph.GA/2305.03758]. <https://doi.org/10.3847/1538-4357/aceda3>.
16. Bellhouse, C.; McGee, S.L.; Smith, R.; Poggianti, B.M.; Jaffé, Y.L.; Kraljic, K.; Franchetto, A.; Fritz, J.; Vulcani, B.; Tonnesen, S.; et al. GASP XXIX - unwinding the arms of spiral galaxies via ram-pressure stripping. *Mon. Not. R. Astron. Soc.* **2021**, *500*, 1285–1312, [arXiv:astro-ph.GA/2010.09733]. <https://doi.org/10.1093/mnras/staa3298>.
17. Schulz, S.; Struck, C. Multi stage three-dimensional sweeping and annealing of disc galaxies in clusters. *Mon. Not. R. Astron. Soc.* **2001**, *328*, 185–202, [arXiv:astro-ph/0107570]. <https://doi.org/10.1046/j.1365-8711.2001.04847.x>.
18. Roediger, E.; Bruggen, M.; Owers, M.S.; Ebeling, H.; Sun, M. Star formation in shocked cluster spirals and their tails. *Mon. Not. R. Astron. Soc.* **2014**, *443*, L114–L118, [arXiv:astro-ph.GA/1405.1033]. <https://doi.org/10.1093/mnrasl/slu087>.
19. Steinhauser, D.; Schindler, S.; Springel, V. Simulations of ram-pressure stripping in galaxy-cluster interactions. *Astron. Astrophys.* **2016**, *591*, A51, [arXiv:astro-ph.GA/1604.05193]. <https://doi.org/10.1051/0004-6361/201527705>.
20. Wolter, A.; Esposito, P.; Mapelli, M.; Pizzolato, F.; Ripamonti, E. NGC 2276: a remarkable galaxy with a large number of ultraluminous X-ray sources. *Mon. Not. R. Astron. Soc.* **2015**, *448*, 781–791, [arXiv:astro-ph.HE/1501.01994]. <https://doi.org/10.1093/mnras/stv054>.
21. Bellhouse, C.; Jaffé, Y.L.; Hau, G.K.T.; McGee, S.L.; Poggianti, B.M.; Moretti, A.; Gullieuszik, M.; Bettoni, D.; Fasano, G.; D'Onofrio, M.; et al. GASP. II. A MUSE View of Extreme Ram-Pressure Stripping along the Line of Sight: Kinematics of the Jellyfish Galaxy JO201. *Astrophys. J.* **2017**, *844*, 49, [arXiv:astro-ph.GA/1704.05087]. <https://doi.org/10.3847/1538-4357/aa7875>.
22. George, K.; Poggianti, B.M.; Gullieuszik, M.; Fasano, G.; Bellhouse, C.; Postma, J.; Moretti, A.; Jaffé, Y.; Vulcani, B.; Bettoni, D.; et al. UVIT view of ram-pressure stripping in action: star formation in the stripped gas of the GASP jellyfish galaxy JO201 in Abell 85. *Mon. Not. R. Astron. Soc.* **2018**, *479*, 4126–4135, [arXiv:astro-ph.GA/1803.06193]. <https://doi.org/10.1093/mnras/sty1452>.
23. Tomičić, N.; Hughes, A.; Kreckel, K.; Renaud, F.; Pety, J.; Schinnerer, E.; Saito, T.; Querejeta, M.; Faesi, C.M.; Garcia-Burillo, S. Two Orders of Magnitude Variation in the Star Formation Efficiency across the Premerger Galaxy NGC 2276. *Astrophys. J. Lett.* **2018**, *869*, L38, [arXiv:astro-ph.GA/1812.05048]. <https://doi.org/10.3847/2041-8213/aaf810>.
24. Vulcani, B.; Poggianti, B.M.; Smith, R.; Moretti, A.; Jaffé, Y.L.; Gullieuszik, M.; Fritz, J.; Bellhouse, C. The Relevance of Ram Pressure Stripping for the Evolution of Blue Cluster Galaxies as Seen at Optical Wavelengths. *Astrophys. J.* **2022**, *927*, 91, [arXiv:astro-ph.GA/2201.02644]. <https://doi.org/10.3847/1538-4357/ac4809>.
25. George, K.; Poggianti, B.M.; Omizzolo, A.; Vulcani, B.; Côté, P.; Postma, J.; Smith, R.; Jaffe, Y.L.; Gullieuszik, M.; Moretti, A.; et al. Candidate ram-pressure stripped galaxies in six low-redshift clusters revealed from ultraviolet imaging. *Astron. Astrophys.* **2024**, *690*, A337, [arXiv:astro-ph.GA/2409.10586]. <https://doi.org/10.1051/0004-6361/202450302>.
26. Krabbe, A.C.; Hernandez-Jimenez, J.A.; Mendes de Oliveira, C.; Jaffe, Y.L.; Oliveira, C.B.; Cardoso, N.M.; Smith Castelli, A.V.; Dors, O.L.; Cortesi, A.; Crossett, J.P. Diagnostic diagrams for ram pressure stripped candidates. *Mon. Not. R. Astron. Soc.* **2024**, *528*, 1125–1141, [arXiv:astro-ph.GA/2312.09220]. <https://doi.org/10.1093/mnras/stad3881>.
27. Crossett, J.P.; Jaffé, Y.L.; McGee, S.L.; Smith, R.; Bellhouse, C.; Bettoni, D.; Vulcani, B.; Kelkar, K.; Lourenço, A.C.C. Identification of ram pressure stripping features in galaxies using citizen science. *Astron. Astrophys.* **2025**, *694*, A204, [arXiv:astro-ph.GA/2412.10060]. <https://doi.org/10.1051/0004-6361/202450371>.
28. Varela-Lavin, S.; Gómez, F.A.; Tissera, P.B.; Besla, G.; Garavito-Camargo, N.; Marinacci, F.; Laporte, C.F.P. Lopsided galaxies in a cosmological context: a new galaxy-halo connection. *Mon. Not. R. Astron. Soc.* **2023**, *523*, 5853–5868, [arXiv:astro-ph.GA/2211.16577]. <https://doi.org/10.1093/mnras/stad1724>.
29. Hernquist, L. An analytical model for spherical galaxies and bulges. *Astrophys. J.* **1990**, *356*, 359–364. <https://doi.org/10.1086/168845>.
30. Springel, V.; Di Matteo, T.; Hernquist, L. Modelling feedback from stars and black holes in galaxy mergers. *Mon. Not. R. Astron. Soc.* **2005**, *361*, 776–794, [arXiv:astro-ph/0411108]. <https://doi.org/10.1111/j.1365-2966.2005.09238.x>.

31. Ruggiero, R.; Lima Neto, G.B. The fate of the gaseous discs of galaxies that fall into clusters. *Mon. Not. R. Astron. Soc.* **2017**, *468*, 4107–4115, [arXiv:1703.08550]. <https://doi.org/10.1093/mnras/stx744>.
32. Springel, V.; Pakmor, R.; Pillepich, A.; Weinberger, R.; Nelson, D.; Hernquist, L.; Vogelsberger, M.; Genel, S.; Torrey, P.; Marinacci, F.; et al. First results from the IllustrisTNG simulations: matter and galaxy clustering. *Mon. Not. R. Astron. Soc.* **2018**, *475*, 676–698, [arXiv:astro-ph.GA/1707.03397]. <https://doi.org/10.1093/mnras/stx3304>.
33. Sellwood, J.A. Spiral Instabilities in N-body Simulations. I. Emergence from Noise. *Astrophys. J.* **2012**, *751*, 44, [arXiv:astro-ph.GA/1203.0444]. <https://doi.org/10.1088/0004-637X/751/1/44>.
34. Sellwood, J.A. Relaxation in N-body Simulations of Disk Galaxies. *Astrophys. J. Lett.* **2013**, *769*, L24, [arXiv:astro-ph.CO/1303.4919]. <https://doi.org/10.1088/2041-8205/769/2/L24>.
35. Nelson, D.; Pillepich, A.; Springel, V.; Pakmor, R.; Weinberger, R.; Genel, S.; Torrey, P.; Vogelsberger, M.; Marinacci, F.; Hernquist, L. First results from the TNG50 simulation: galactic outflows driven by supernovae and black hole feedback. *Mon. Not. R. Astron. Soc.* **2019**, *490*, 3234–3261, [arXiv:astro-ph.GA/1902.05554]. <https://doi.org/10.1093/mnras/stz2306>.
36. Habibi, A.; Roshan, M.; Hosseinirad, M.; Khosroshahi, H.; Aguerri, J.A.L.; Cuomo, V.; Abbassi, S. The redshift evolution of galactic bar pattern speed in TNG50. *Astron. Astrophys.* **2024**, *691*, A122, [arXiv:astro-ph.GA/2409.02456]. <https://doi.org/10.1051/0004-6361/202451028>.
37. Fragkoudi, F.; Grand, R.J.J.; Pakmor, R.; Springel, V.; White, S.D.M.; Marinacci, F.; Gomez, F.A.; Navarro, J.F. Revisiting the tension between fast bars and the Λ CDM paradigm. *Astron. Astrophys.* **2021**, *650*, L16, [arXiv:astro-ph.GA/2011.13942]. <https://doi.org/10.1051/0004-6361/202140320>.
38. Springel, V. The cosmological simulation code GADGET-2. *Mon. Not. R. Astron. Soc.* **2005**, *364*, 1105–1134, [arXiv:astro-ph/0505010]. <https://doi.org/10.1111/j.1365-2966.2005.09655.x>.
39. Stark, D.V.; Bundy, K.A.; Westfall, K.; Bershad, M.; Weijmans, A.M.; Masters, K.L.; Kruk, S.; Brinchmann, J.; Soler, J.; Abraham, R.; et al. SDSS-IV MaNGA: characterizing non-axisymmetric motions in galaxy velocity fields using the Radon transform. *Mon. Not. R. Astron. Soc.* **2018**, *480*, 2217–2235, [arXiv:astro-ph.GA/1807.11503]. <https://doi.org/10.1093/mnras/sty1991>.
40. Krone-Martins, A.; Ducourant, C.; Teixeira, R.; Galluccio, L.; Gavras, P.; dos Anjos, S.; de Souza, R.E.; Machado, R.E.G.; Le Campion, J.F. Pushing the limits of the Gaia space mission by analyzing galaxy morphology. *Astron. Astrophys.* **2013**, *556*, A102, [arXiv:astro-ph.IM/1307.5732]. <https://doi.org/10.1051/0004-6361/201219697>.
41. Roediger, E.; Brüggen, M. Ram pressure stripping of disc galaxies orbiting in clusters - I. Mass and radius of the remaining gas disc. *Mon. Not. R. Astron. Soc.* **2007**, *380*, 1399–1408, [arXiv:astro-ph/0707.2698]. <https://doi.org/10.1111/j.1365-2966.2007.12241.x>.
42. Smith, R.; Fellhauer, M.; Assmann, P. Ram pressure drag - the effects of ram pressure on dark matter and stellar disc dynamics. *Mon. Not. R. Astron. Soc.* **2012**, *420*, 1990–2005, [arXiv:astro-ph.CO/1110.5555]. <https://doi.org/10.1111/j.1365-2966.2011.20077.x>.
43. Tonnesen, S. The Journey Counts: The Importance of Including Orbits when Simulating Ram Pressure Stripping. *Astrophys. J.* **2019**, *874*, 161, [arXiv:astro-ph.GA/1903.08178]. <https://doi.org/10.3847/1538-4357/ab0960>.

Disclaimer/Publisher’s Note: The statements, opinions and data contained in all publications are solely those of the individual author(s) and contributor(s) and not of MDPI and/or the editor(s). MDPI and/or the editor(s) disclaim responsibility for any injury to people or property resulting from any ideas, methods, instructions or products referred to in the content.